Electronic Supplementary Material (ESI) for Journal of Materials Chemistry C.
This journal is © The Royal Society of Chemistry 2018

Supplementary Information

Er^{3+}/Yb^{3+} codoped phosphor $Ba_3Y_4O_9$ with intense red upconversion emission and optical temperature sensing behavior

Hao Wu,[a,b] Zhendong Hao,[a*] Liangliang Zhang,[a] Xia Zhang,[a] Yu Xiao,[a,b] Guo-Hui Pan,[a] Huajun Wu,[a] Yongshi Luo,[a] Ligong Zhang[a] and Jiahua Zhang[a*]

[a] State Key Laboratory of Luminescence and Applications, Changchun Institute of Optics, Fine Mechanics and Physics, Chinese Academy of Sciences, Changchun, 130033, China

[b] University of Chinese Academy of Sciences, Beijing, 100049, China

Corresponding author*

Email: haozd@ciomp.ac.cn; zhangjh@ciomp.ac.cn

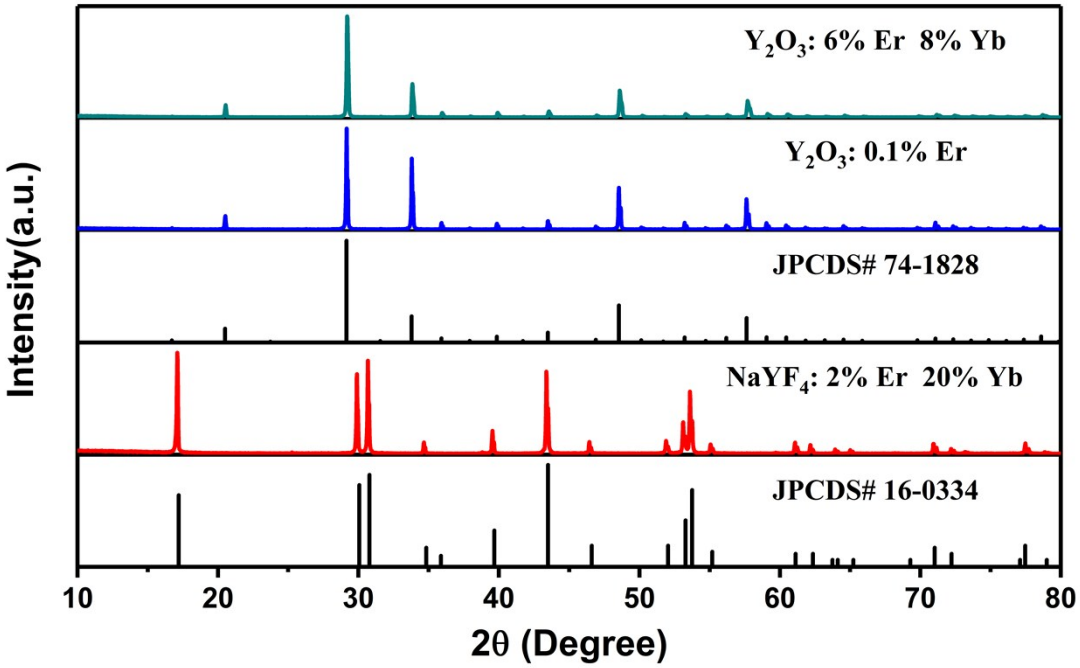

Fig. S1 X-ray diffraction patterns of Y_2O_3 and β-$NaYF_4$ with particular Er^{3+}, Yb^{3+} doped or codoped concentration. The standard patterns are also presented as references.

Evaluating emission efficiency of $^4F_{9/2}$ level and radiative lifetime in $Ba_3Y_4O_9$.

The PL spectra of $Ba_3Y_4O_9$ and Y_2O_3 with the singly 0.1%Er^{3+} doped concentration were recorded under 650nm excitation in **Figure 5a**, and the full spectra shape of red emission are also presented (red dashed line). We simplify the scheme of possible decay pathways by assuming that $^4I_{9/2}$ level can rapidly and completely relax down to $^4I_{11/2}$ level by multiphonon-relaxation (MPR) due to the small energy gap of ~2200cm^{-1}. There is no MPR process from $^4I_{13/2}$ level due to the large energy gap ~6500cm^{-1}, which is five times larger than the maximum phonon energy in oxide hosts. According to the previously reported radiative branch ratios from $^4F_{9/2}$ to various lower states of Er^{3+} in various hosts,[1-15] $^4F_{9/2}\rightarrow{}^4I_{15/2}$ is the dominant radiative transition with the branch ratio around 91% ($\beta_{40}\approx0.91$), while the others $^4F_{9/2}\rightarrow{}^4I_{13/2}$ ($\beta_{41}\approx0.05$) and $^4F_{9/2}\rightarrow{}^4I_{11/2}$ ($\beta_{41}\approx0.04$) can be nearly neglected. Under direct excitation to $^4F_{9/2}$ at 650nm, the set of rate equations are expressed below using the model portrayed in **Figure 5b**:

$$\frac{dn_4}{dt} = \sigma_4\Phi_{650}n_0 - \alpha_4n_4 - W_4n_4 \quad \text{(S1)}$$

$$\frac{dn_3}{dt} = \alpha_{43}n_4 + W_4n_4 - W_3n_3 \quad \text{(S2)}$$

$$\frac{dn_2}{dt} = \alpha_{42}n_4 + W_3n_3 - \alpha_2n_2 - W_2n_2 \quad \text{(S3)}$$

$$\frac{dn_1}{dt} = \alpha_{41}n_4 + \alpha_{21}n_2 + W_2n_2 - \alpha_1n_1 \quad \text{(S4)}$$

$$1 = \sum\beta_{ij} \quad (i > j) \quad \text{(S5)}$$

$$\alpha_{ij} = \alpha_i\beta_{ij} \quad \text{(S6)}$$

where n_i is the population of level i, σ_4 is the absorption cross section of $^4F_{9/2}$, and Φ_{650} is the excitation photon flux. The β_{ij} is the branching ratio from the ith level to the jth level. The α_i and W_i represent the radiative rate and MPR rate of ith level, respectively. Considering the low efficiency of red emission in oxide and the largest radiative branch ratios of $^4F_{9/2}\rightarrow{}^4I_{15/2}$ transition, the contribution of radiative transition from $^4F_{9/2}$ to each intermediate states can be ignored. Furthermore, the PL spectra were measured by continuous wave (CW) excitation, thus the steady state equations are expressed as:

$$\sigma_4\Phi_{650}n_0 = \alpha_4n_4 + W_4n_4 \quad \text{(S7)}$$

$$W_4 n_4 = W_3 n_3 \tag{S8}$$

$$W_3 n_3 = \alpha_2 n_2 + W_2 n_2 \tag{S9}$$

$$\alpha_1 n_1 = \alpha_{21} n_2 + W_2 n_2 \tag{S10}$$

The PL intensity (I) is proportional to the product of radiative rate and the population of emitting state:

$$I_{ij} \propto \alpha_{ij} n_i \tag{S11}$$

where I_{ij} is transition integrated intensity from the *i*th level to the *j*th level. Further, the $^4I_{13/2} \rightarrow {}^4I_{15/2}$ and $^4I_{11/2} \rightarrow {}^4I_{15/2}$ transition intensity ratio can be expressed as:

$$\frac{I_{10}}{I_{20}} = \frac{(\alpha_{21} n_2 + W_2 n_2)}{\alpha_{20} n_2} \times R_{1500/1000} = \left(\frac{\beta_{21}}{\beta_{20}} + \frac{W_2}{\alpha_2 \beta_{20}}\right) \times R_{1500/1000} \tag{S12}$$

where, $R_{1500/1000}$ is the coefficient for detector response and transition frequency ratio of 1500nm to 1000nm. According to the theoretical calculation of different Er^{3+} doped hosts previously (**Table S1**), the branching ratio of $^4I_{11/2}$ and $^4F_{9/2}$ level in different host materials are approximately identical. Thus, we regard the average values of composite oxide as the branching ratio of $^4I_{11/2}$ and $^4F_{9/2}$ level in $Ba_3Y_4O_9$. Taking Y_2O_3 sample as a reference, the evaluated radiative lifetime and luminescence efficiency of $^4I_{11/2}$ level were obtained using the equation:

$$\eta_i = \frac{\tau_i}{\tau_{i\,r}} = \frac{\alpha_i}{\alpha_i + W_i} \tag{S13}$$

where η_i is the luminescence efficiency of *i*th level, τ_i is the experimental lifetime (τ_{exp}) and τ_{ir} is the calculated radiative lifetime (τ_{cal}) or evaluated radiative lifetime (τ_{eva}) .

Moreover, the $^4I_{11/2} \rightarrow {}^4I_{15/2}$ and $^4F_{9/2} \rightarrow {}^4I_{15/2}$ transition intensity ratio can be expressed as:

$$\frac{I_{20}}{I_{40}} = \frac{\alpha_{20} W_4 n_4/(\alpha_2 + W_2)}{\alpha_{40} n_4} R_{1000/650} = \frac{W_4}{\alpha_4 \beta_{40}} \times \eta_2 \times \beta_{20} \times R_{1000/650} \tag{S14}$$

where $R_{1000/650}$ is the coefficient for detector response and transition frequency ratio of 1000nm to 650nm. Taking Y_2O_3 sample as a reference, the evaluated radiative lifetime and luminescence efficiency of $^4F_{9/2}$ were obtained using **Equation S13** and the detailed parameters are listed in **Table S2,3**.

Table S1. Comparison of branching ratio reported for $^4I_{11/2}$ and $^4F_{9/2}$ level of Er^{3+} in different host materials.

	β_{21}(%)	β_{20}(%)	β_{43}(%)	β_{42}(%)	β_{41}(%)	β_{40}(%)	Ref
K_2YF_5	28.7	71.3	0.2	3.9	4.2	91.7	1
β-$NaYF_4$	16.2	83.8	0.6	8.4	3.8	87.2	2
KPb_2Cl_5	18.4	81.6	0	3.8	4.2	92.0	3
$CaGdAlO_4$	15.8	84.2	0.3	3.8	4.4	91.5	4
$ErBa_3B_9O_{18}$	13	87	0	6	4	90	5
Y_2O_3	10.8	89.2	2.1	0.8	4.8	92.3	6
$CaSc_2O_4$	18.7	81.2	0.3	3.7	4.8	91.2	7
Gd_2SiO_5	16.1	83.9	0.2	3.8	4.8	91.2	8
$KGd(WO_4)_2$	20.4	79.6	0.7	5.7	5.5	88.1	9
$Li_2Gd_4(MoO_4)_7$	13.7	86.3	0.8	4.1	5.8	89.3	10
$Sr_3Y(BO_3)_3$	21.6	78.4	0.2	2.8	4.5	92.5	11
Y_2O_2S	13.5	86.5	0.2	5.1	4.6	90.1	12
YAG	-	-	0.1	6.8	3.3	89.8	13
$YAl_3(BO_3)_4$	12.9	87.1	0.2	4.1	4.5	91.2	14
$YAlO_3$	14.5	85.5	0.2	4.3	4.0	91.5	15
Oxide mean	15.5	84.5	0.4	4.3	4.6	90.7	

Table S2. The detailed parameters for evaluating radiative lifetime and luminescence efficiency of $^4I_{11/2}$ level in $Ba_3Y_4O_9$.

0.1%Er	β_{21}(%)	β_{20}(%)	τ_{rad} (ms)	τ_{exp} (ms)	I_{10}/I_{20}	τ_{eva} (ms)	η_2(%)
$Ba_3Y_4O_9$	~15.5[a)]	~84.5[a)]	-	1.852	$1.29I_{1/2}$[b)]	4.700	39.66
Y_2O_3	10.8	89.2	6.032	2.669	$I_{1/2}$[b)]	-	44.25

[a)] Using the average values of composite oxide in **Table S1**.

[b)] $I_{1/2}$ represents the $^4I_{13/2}\rightarrow{}^4I_{15/2}$ and $^4I_{11/2}\rightarrow{}^4I_{15/2}$ transition intensity ratio in Y_2O_3:0.1%Er^{3+}

Table S3. The detailed parameters for evaluating radiative lifetime and luminescence efficiency of $^4F_{9/2}$ level in $Ba_3Y_4O_9$.

0.1%Er	β_{40}(%)	τ_{rad} (μs)	τ_{exp} (μs)	I_{20}/I_{40}	τ_{eva} (μs)	η_4(%)
$Ba_3Y_4O_9$	~90.7[a)]	-	31.61	$0.66I_{2/4}$[b)]	879.28	3.595
Y_2O_3	92.3	737.53	20.33	$I_{2/4}$[b)]	-	2.756

[a)] Using the average values of composite oxide in **Table S1**.

[b)] $I_{2/4}$ represents the $^4I_{11/2}\rightarrow{}^4I_{15/2}$ and $^4F_{9/2}\rightarrow{}^4I_{15/2}$ transition intensity ratio in Y_2O_3:0.1%Er^{3+}

References

[1] P. A. Loiko, E. V. Vilejshikova, N. M. Khaidukov, M. N. Brekhovskikh, X. Mateos, M. Aguiló, K. V. Yumashev, *J. Lumin*., 2016, **180**, 103.

[2] G. Yao, C. Lin, Q. Meng, P. S. May, M. T. Berry, *J. Lumin*., 2015, **160**, 276.

[3] N. W. Jenkins, S. R. Bowman, S. O'Connor, S. K. Searles, J. Ganem, *Opt. Mater*., 2003, **22**, 311.

[4] J. H. Huang, X. H. Gong, Y. J. Chen, Y. F. Lin, Z. D. Luo, Y. D. Huang, *J. Alloy. Compd*., 2014, **585**, 163.

[5] M. He, T. Liu, J. Xiu, Y. Tang, Z. Zhang, *J. Spectrosc*., 2015, 871320.

[6] D. K. Sardar, K. L. Nash, R. M. Yow, G. B. Gruber, *J. Appl. Phys*., 2007, **101**, 113115.

[7] Ş. Georgescu, A. Ştefan, O. Toma, *J. Lumin*., 2015, **167**, 186.

[8] X. Xu, G. Zhao, F. Wu, W. Xu, Y. Zong, X. Wang, Z. Zhao, G. Zhou, J. Xu, *J. Cryst. Growth*., 2008, **310**, 156.

[9] M. C. Pujol, M. Rico, C. Zaldo, R. Solé, V. Nikolov, X. Solans, M. Aguiló, F. Díaz, *Appl. Phys. B-Lasers O*., 1999, **68**, 187-197.

[10] W. Zhao, L. Zhang, G. Wang, *J. Cryst. Growth*., 2009, **311**, 2336.

[11] D, Zhao, G, Wang, *J. Lumin*., 2010, **130**, 424.

[12] S. Buddhudu, F. J. Bryant, *J. Less-Common Met*., 1989, **147**, 213.

[13] D. K. Sardar, W. M. Bradley, J. J. Perez, J. B. Gruber, B. Zandi, J. A. Hutchinson, C. W. Trussell, M. R. Kokta, *J. Appl. Phys*., 2003, **93**, 2602.

[14] H. Jiang, J. Wang, X. Hu, H. Liu, X. Y. Liu, *Chem. Phys. Lett*., 2002, **365**, 279.

[15] Q. Dong, G. Zhao, D. Cao, J. Chen, Y. Ding, *J. Alloy. Compd*., 2010, **493**, 661.